International Journal of Heat and Mass Transfer 54 (2011) 3081–3089

Contents lists available at ScienceDirect

International Journal of Heat and Mass Transfer

journal homepage: www.elsevier.com/locate/ijhmt

The onset of convection in porous layers with multiple horizontal partitions

D. Andrew S. Rees [a,*], Gamze Genç [a,b]

[a] Mechanical Engineering, University of Bath, Bath BA2 7AY, UK
[b] Mechanical Engineering, University of Erciyes, 38039 Kayseri, Turkey

ARTICLE INFO

Article history:
Received 24 August 2010
Accepted 28 January 2011

Keywords:
Partitioned porous layer
Onset of convection
Critical Darcy–Rayleigh number
Dispersion relation
Asymptotic analysis

ABSTRACT

In this paper we investigate the onset of convection in a horizontally partitioned porous layer which is heated from below. Identical sublayers are separated by thin impermeable barriers. A linear stability analysis is performed, and dispersion relations are obtained directly and explicitly for two- and three-layer configurations. A systematic numerical procedure is devised to compute the dispersion relation for an arbitrary number of sublayers, but from this it is possible to guess the correct analytical form of the dispersion relation for general cases.

Neutral stability curves are found to organise themselves into natural groups of N members when there are N sublayers. When the disturbance wavenumber, k, is large, each member of any group lies within an $O(k^{-1})$ distance of all other members, but within an $O(1)$ distance of other groups. When the number of sublayers is large, the system tends towards one with a critical Darcy–Rayleigh number of 12 and a critical wavenumber of zero; this is the well-known property of a single porous layer with constant heat flux boundary conditions. An asymptotic analysis is performed in order explore these two apparently disparate configurations. Finally, another asymptotic analysis is used to determine the critical Rayleigh number and its associated wavenumber when the number of sublayers is large.

1. Introduction

In the present paper we consider the onset of convection within a horizontal porous layer heated from below which has multiple infinitesimally thin impermeable horizontal partitions embedded within it. The resulting sublayers are then identical in all respects, including their height. Thus the sublayers are mechanically decoupled but remain thermally coupled since the interfaces present no barrier to the conduction of heat. This work forms an extension to our previous paper [1] which was concerned with a two-layer system.

Many authors have considered how the presence of layering affects the onset of convection and the subsequent nonlinear cellular flow. Being motivated mostly by geothermal applications, these layered systems generally tend to have interfaces though which fluid may flow, unlike the topic of the present paper. The first person to consider layering was Georghitza [2] who considered weak layering in the sense that the difference in the permeabilities of the two layers was small. On the other hand, Donaldson [3] considered a two-layer system where one of the sublayers is impermeable and computed nonlinear two-dimensional flow patterns. Riahi [4] considered what might be termed a three-layer configuration where a porous layer is sandwiched between two impermeable but conducting regions of infinite height. He conducted a weakly nonlinear analysis and found that there is a region in parameter space within which two-dimensional rolls do not form the favoured convection pattern; this role is passed to a square-cell pattern. Further analyses of this type may be found in Mojtabi and Rees [5] and Rees and Mojtabi [6]. Masuoka et al. [7] provided some criteria for the onset of convection in a two-layer configuration where both sublayers are porous, and Rana et al. [8] conducted a numerical study of a three-layer configuration which was believed to model well the Pahoa reservoir in Hawaii.

A more systematic approach to these problems was provided in the 1980s by McKibbin and co-workers who provided comprehensive data on the onset problem [9], post-critical heat transfer [10], the effects of thin highly permeable cracks [11] and almost impermeable sheets [12]. Indeed, the present paper may also be regarded as an extension of [12] to the case where the sheets are completely impermeable. Jang and Tsai [13] considered a three-layer system where the middle sublayer is impermeable but conducting, and of finite thickness. They showed that the system is at its most stable when the partition is located centrally, and the system also becomes more stable as the partition thickness increases or the partition conductivity decreases. The paper by Postelnicu [14] is also of relevance.

Of some interest is the fact that the presence of layering can cause the neutral stability curve to adopt a shape other than that

* Corresponding author at: Mechanical Engineering, University of Bath, Bath BA2 7AY, UK.
E-mail address: ensdasr@bath.ac.uk (D.A.S. Rees).

0017-9310/$ - see front matter © 2011 Elsevier Ltd. All rights reserved.
doi:10.1016/j.ijheatmasstransfer.2011.02.002

Nomenclature

A, B, C, D	constants
c	constant in Eq. (43)
$\underline{d}$	vector
f, g	reduced forms of perturbations
$\mathcal{F}$	the dispersion relation
$\hat{g}$	gravity
H	height of each sublayer
k	disturbance wavenumber
$\hat{k}$	scaled value of k
K	permeability
$\mathcal{M}, \mathcal{N}$	4×4 matrices
N	number of sublayers
p	pressure
Ra	Darcy–Rayleigh number
S	scaled value of Ra
t	time
u	horizontal velocity
$\underline{v}$	vector of coefficients
w	vertical velocity
x	horizontal coordinate
z	vertical coordinate

Greek symbols

α	exponent
β	thermal expansion coefficient
δ	equal to $N^{-1/2}$
ΔT	reference temperature drop
θ	temperature
Θ	disturbance temperature
κ	thermal diffusivity
λ, σ	constants
μ	dynamic viscosity
ρ	density
ψ	streamfunction
Ψ	disturbance streamfunction

Subscripts and superscripts

(b)	basic state
c	critical conditions
j	sublayer index
m	iteration number
$'$	derivative with respect to z
$1,2,\ldots$	pertaining to a sublayer

with the classical single minimum. McKibbin and O'Sullivan [9] found cases where the neutral curve has a double minimum, and it is often the case that a small change in a system parameter (such as the permeability of one of the sublayers) causes a discontinuous change in the critical wavenumber; this is due to the neutral curve having two minima and the small change in the parameter has simply caused the identity of the mode with the smaller Rayleigh number to swap from one wavenumber to the other. Rees and Riley [15] provided a systematic analysis of two- and three-layer configurations and they traced out the locus in parameter space where such bimodality arises. They also found that it is possible to have three-layer configurations which are trimodal, i.e. that three minima exist each having the same Rayleigh number. Moreover, they also determined regions in parameter space where square-cell convection forms the stable pattern.

In the present paper we will be considering the onset of convection in a porous layer where the layering is brought about by having equally-spaced infinitesimally thin horizontal partitions within the layer. Thus all the sublayers are identical in all of their properties. Such a configuration is an extension of the recent work by Genç and Rees [1] who considered a two-layer system. Much of the analysis we present arises from the dispersion relation which may be calculated by hand fairly easily for two- and three-layer systems, but which may be computed easily for larger numbers of sublayers. It is found that this type of layered system has some unusual properties, namely (i) the neutral curves clump together into groups of N curves when there are N sublayers; (ii) that the curves comprising each group lie within an $O(k^{-1})$ distance of one another when the wavenumber, k, is large; (iii) the critical Darcy–Rayleigh number and wavenumber for the first mode tend towards the respective values 12 and 0 as the number of sublayers increases, which corresponds to the single-layer values when constant heat flux boundary conditions are applied.

2. Governing equations

We consider the onset of convection in a horizontal porous layer which is comprised of a number of identical sublayers which are themselves separated by infinitesimally thin impermeable partitions. Therefore, while fluid may not pass between sublayers, conductive heat transfer is unhindered by the presence of these partitions. A five-sublayer version of the configuration we consider is shown in Fig. 1.

We will assume that the Boussinesq approximation is valid, that the porous medium is homogeneous and isotropic, that the phases are in local thermal equilibrium, and that the fluid motion satisfies Darcy's law with the additional effect of buoyancy. Each sublayer has height, H, which means that a system comprised of N sublayers has height, NH. We will use H as the value against which to nondimensionalise the governing equations, rather than NH; this has the advantage of yielding much easier comparisons between cases which consist of different numbers of sublayers, particularly the classical single-layer Darcy–Bénard problem.

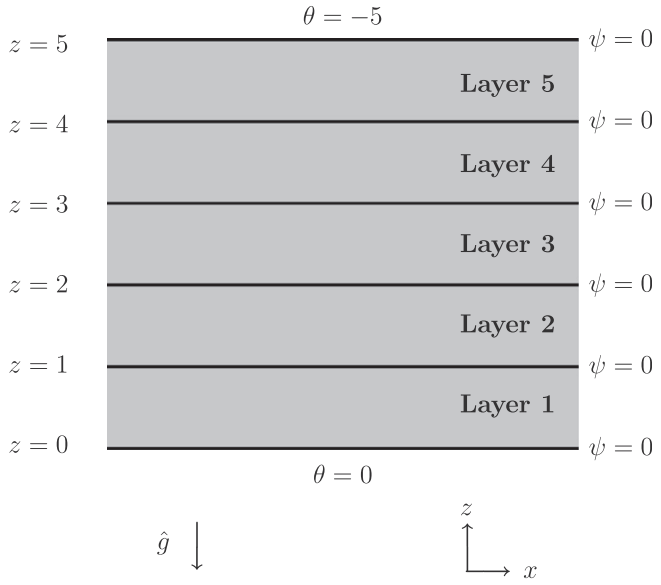

Fig. 1. Depicting a horizontally layered porous medium consisting of five sublayers.

Given that we are considering a linear stability analysis in a horizontally unbounded layer, and given that all three-dimensional modes in this type of stability problem may be decomposed into two-dimensional roll cells, we shall present our analysis in terms of two-dimensional equations. The full governing equations in nondimensional form are given by

$$\frac{\partial u_j}{\partial x}+\frac{\partial w_j}{\partial z}=0, \tag{1}$$

$$u_j=-\frac{\partial p_j}{\partial x},\quad w_j=-\frac{\partial p_j}{\partial z}+\mathrm{Ra}\,\theta_j, \tag{2}$$

$$\frac{\partial \theta_j}{\partial t}+u_j\frac{\partial \theta_j}{\partial x}+w_j\frac{\partial \theta_j}{\partial z}=\frac{\partial^2\theta_j}{\partial x^2}+\frac{\partial^2\theta_j}{\partial z^2}, \tag{3}$$

where all quantities are given in the Nomenclature, where $j = 1,2,\ldots,N$ denotes the identity of the sublayer which is being considered, and where N is the number of sublayers. In the above equations, Ra is the Darcy–Rayleigh number given by

$$\mathrm{Ra}=\frac{\rho\hat{g}\beta HK\Delta T}{\mu\kappa}, \tag{4}$$

and ΔT is the basic temperature drop across a single sublayer. We note that, if we had used the overall height of the layer and the total temperature drop as the respective length and temperature scales in the nondimensionalisation, then the corresponding Darcy–Rayleigh number would be a factor of N^2 larger than the one given in Eq. (4).

The streamfunction, ψ, is defined using,

$$u_j=-\frac{\partial \psi_j}{\partial z},\quad w_j=\frac{\partial \psi_j}{\partial x}, \tag{5}$$

and therefore the non-dimensional equations take the following forms:

$$\frac{\partial^2\psi_j}{\partial x^2}+\frac{\partial^2\psi_j}{\partial z^2}=\mathrm{Ra}\frac{\partial\theta_j}{\partial x},\quad \frac{\partial\theta_j}{\partial t}+\frac{\partial\psi_j}{\partial x}\frac{\partial\theta_j}{\partial z}-\frac{\partial\psi_j}{\partial z}\frac{\partial\theta_j}{\partial x}=\frac{\partial^2\theta_j}{\partial x^2}+\frac{\partial^2\theta_j}{\partial z^2}. \tag{6}$$

These equations are to be solved subject to the boundary and interface conditions,

$$\begin{aligned} &z=0: \quad \psi_1=0,\quad \theta_1=0,\\ &z=j: \quad \psi_j=\psi_{j+1}=0,\quad \theta_j=\theta_{j+1},\quad \tfrac{\partial\theta_j}{\partial z}=\tfrac{\partial\theta_{j+1}}{\partial z},\quad (j=1,\ldots,N-1),\\ &z=N: \quad \psi_N=0,\quad \theta_N=-N. \end{aligned} \tag{7}$$

3. Linear stability analysis

3.1. Perturbation equations

The basic state which we analyse for stability is one with no flow and a linear temperature drop:

$$\theta_j^{(b)}=-z,\quad \psi_j^{(b)}=0\quad (j=1,\ldots,N). \tag{8}$$

Disturbances are introduced by substituting,

$$\psi_j=\psi_j^{(b)}+\Psi_j,\quad \theta_j=\theta_j^{(b)}+\Theta_j, \tag{9}$$

into Eq. (6), and then linearising to find the governing equations for Ψ_j and Θ_j:

$$\frac{\partial^2\Psi_j}{\partial x^2}+\frac{\partial^2\Psi_j}{\partial z^2}=\mathrm{Ra}\frac{\partial\Theta_j}{\partial x},\quad \frac{\partial\Theta_j}{\partial t}-\frac{\partial\Psi_j}{\partial x}=\frac{\partial^2\Theta_j}{\partial x^2}+\frac{\partial^2\Theta_j}{\partial z^2}. \tag{10}$$

These perturbation equations may be proved to be self-adjoint, and therefore the onset of convection is stationary, and we may neglect the time-derivative term in Eq. (10). We may also factor out a horizontal Fourier mode with wavenumber, k, by setting,

$$\Psi_j=f_j(z)\cos kx,\quad \Theta_j=g_j(z)\sin kx. \tag{11}$$

Eq. (10) now become,

$$f_j''-k^2f_j=\mathrm{Ra}\,kg_j,\quad g_j''-k^2g_j=kf_j, \tag{12}$$

and are subject to the boundary and interface conditions,

$$\begin{aligned} &z=0: \quad f_1=g_1=0,\\ &z=j: \quad f_j=0,\quad g_j=g_{j+1},\quad g_j'=g_{j+1}',\quad (j=1,\ldots,N-1)\\ &z=N: \quad f_N=g_N=0. \end{aligned} \tag{13}$$

Eqs. (12) and (13) now represent an eigenvalue problem for Ra in terms of k.

The analysis for the onset of convection in a single layer is well-known, but is repeated here in a slightly different fashion (i.e. by determining a dispersion relation) so that the analysis might be extended easily for multiple sublayers.

3.2. Single layer analysis

Eq. (12) form a linear constant-coefficient system, and therefore all possible complementary function solutions take the form, $e^{\alpha z}$, for which 4 possible values of α may be found for all possible values of Ra and k. Therefore the solutions to these equations in layer 1 may be written in the form,

$$f_1=\mathrm{Ra}^{1/2}[A_1\sinh\lambda z+B_1\cosh\lambda z+C_1\sin\sigma z+D_1\cos\sigma z], \tag{14}$$

$$g_1=A_1\sinh\lambda z+B_1\cosh\lambda z-C_1\sin\sigma z-D_1\cos\sigma z. \tag{15}$$

In these equations the constants, A_1, B_1, C_1 and D_1 are presently arbitrary, while λ and σ are defined according to,

$$\lambda=(k\mathrm{Ra}^{1/2}+k^2)^{1/2},\quad \sigma=(k\mathrm{Ra}^{1/2}-k^2)^{1/2}. \tag{16}$$

For a single layer, we have four boundary conditions to satisfy, namely,

$$f_1(0)=g_1(0)=f_1(1)=g_1(1)=0, \tag{17}$$

and substitution of all of these into Eqs. (14) and (15) yields the following,

$$\begin{pmatrix} 0 & 1 & 0 & 1\\ \sinh\lambda & \cosh\lambda & \sin\sigma & \cos\sigma\\ 0 & 1 & 0 & -1\\ \sinh\lambda & \cosh\lambda & -\sin\sigma & -\cos\sigma \end{pmatrix}\begin{pmatrix} A_1\\ B_1\\ C_1\\ D_1 \end{pmatrix}=\begin{pmatrix} 0\\ 0\\ 0\\ 0 \end{pmatrix}. \tag{18}$$

The first and third of the equations given in (18) yield $B_1 = D_1 = 0$, while the second gives $A_1\sinh\lambda = 0$ from which we conclude that $A_1 = 0$. Finally, the fourth yields the dispersion relation for the one-layer system, namely,

$$\sin\sigma=0, \tag{19}$$

while C_1 naturally remains arbitrary. Eq. (19) is equivalent to the familiar expression for the Darcy–Bénard neutral curve, namely,

$$\mathrm{Ra}=\frac{(k^2+n^2\pi^2)^2}{k^2}. \tag{20}$$

Here, mode n consists of n vertically stacked contra-rotating rolls, and $n = 1$ yields the mode with the lowest critical Rayleigh number, namely $\mathrm{Ra}_c = 4\pi^2$ and $k_c = \pi$.

3.3. Analysis for an arbitrary number of sublayers

The most convenient form for expressing the solutions in other sublayers is the following,

$$f_j(z)=\mathrm{Ra}^{1/2}\left[A_j\sinh\lambda z_j+B_j\cosh\lambda z_j+C_j\sin\sigma z_j+D_j\cos\sigma z_j\right], \tag{21}$$

$$g_j(z)=A_j\sinh\lambda z_j+B_j\cosh\lambda z_j-C_j\sin\sigma z_j-D_j\cos\sigma z_j, \tag{22}$$

where $z_j = z-(j-1)$ lies in the range, $0\leqslant z_j\leqslant 1$, in sublayer j.

In sublayer 1 we have the following three boundary conditions,

$$f_1(0) = 0, \quad f_1(1) = 0, \quad g_1(0) = 0, \tag{23}$$

which translates into the matrix/vector form,

$$\begin{pmatrix} 0 & 1 & 0 & 1 \\ \sinh\lambda & \cosh\lambda & \sin\sigma & \cos\sigma \\ 0 & 1 & 0 & -1 \end{pmatrix} \begin{pmatrix} A_1 \\ B_1 \\ C_1 \\ D_1 \end{pmatrix} = \begin{pmatrix} 0 \\ 0 \\ 0 \end{pmatrix}. \tag{24}$$

It is again straightforward to show that $B_1 = D_1 = 0$, as for the single layer. Eq. (24) also yields the relation,

$$A_1 \sinh\lambda + C_1 \sin\sigma = 0, \tag{25}$$

for which we adopt the solution,

$$A_1 = \sin\sigma, \quad C_1 = -\sinh\lambda. \tag{26}$$

Therefore we may write the solution for sublayer 1 in the form,

$$\underline{v}_1 = \begin{pmatrix} A_1 \\ B_1 \\ C_1 \\ D_1 \end{pmatrix} = \begin{pmatrix} \sin\sigma \\ 0 \\ -\sinh\lambda \\ 0 \end{pmatrix}, \tag{27}$$

where we define $\underline{v}_j = (A_j, B_j, C_j, D_j)^T$ for simplicity of notation.

Now we need to consider the boundary conditions for f in sublayer $j+1$ and the thermal interface conditions between sublayers j and $j+1$:

$$f_{j+1}(j) = 0, \quad f_{j+1}(j+1) = 0, \quad g_j(j) = g_{j+1}(j), \quad g_j'(j) = g_{j+1}'(j). \tag{28}$$

These conditions may be translated into matrix/vector form, as follows,

$$\begin{pmatrix} 0 & 1 & 0 & 1 \\ \sinh\lambda & \cosh\lambda & \sin\sigma & \cos\sigma \\ 0 & 1 & 0 & -1 \\ \lambda & 0 & -\sigma & 0 \end{pmatrix} \begin{pmatrix} A_{j+1} \\ B_{j+1} \\ C_{j+1} \\ D_{j+1} \end{pmatrix} = \begin{pmatrix} 0 & 0 & 0 & 0 \\ 0 & 0 & 0 & 0 \\ \sinh\lambda & \cosh\lambda & -\sin\sigma & -\cos\sigma \\ \lambda\cosh\lambda & \lambda\sinh\lambda & -\sigma\cos\sigma & \sigma\sin\sigma \end{pmatrix} \begin{pmatrix} A_j \\ B_j \\ C_j \\ D_j \end{pmatrix}, \tag{29}$$

and they may, in turn, also be expressed in the more compact form,

$$\mathcal{M}\underline{v}_{j+1} = \mathcal{N}\underline{v}_j. \tag{30}$$

Thus it is possible to solve for $\underline{v}_{j+1}$ in terms of $\underline{v}_j$, and therefore the solution in the uppermost sublayer, sublayer N, may be written in the form,

$$\underline{v}_N = (\mathcal{M}^{-1}\mathcal{N})^{N-1}\underline{v}_1. \tag{31}$$

Finally, the upper surface boundary condition for g_N, which is the final boundary condition to be applied, takes the simple form that $g_N(N) = 0$. This may be written in the form,

$$(\sinh\lambda \quad \cosh\lambda \quad -\sin\sigma \quad -\cos\sigma) \begin{pmatrix} A_2 \\ B_2 \\ C_2 \\ D_2 \end{pmatrix} = 0. \tag{32}$$

If we define the row vector, $\underline{d} = (\sinh\lambda, \cosh\lambda, -\sin\sigma, -\cos\sigma)$, then the application of this last boundary condition yields an expression for the desired dispersion relation:

$$\underline{d} \cdot \underline{v}_N = \underline{d} \cdot \left[(\mathcal{M}^{-1}\mathcal{N})^{N-1}\right] \cdot \underline{v}_1 = 0. \tag{33}$$

This is a relatively simple formula to encode, and the task is made even simpler when one recognises that the inversion of $\mathcal{M}$ may be replaced by the inversion of two 2×2 matrices instead.

The appropriate dispersion relation for two sublayers is quite quick to determine on paper, and the above formula gives precisely the following expression,

$$4\sin\sigma\sinh\lambda(\lambda\cosh\lambda\sin\sigma + \sigma\cos\sigma\sinh\lambda) = 0. \tag{34}$$

Therefore neutral stability corresponds to when either

$$\sin\sigma = 0, \quad \text{or} \quad \lambda\sin\sigma\cosh\lambda + \sigma\sinh\lambda\cos\sigma = 0 \tag{35}$$

the former of which is the single-layer (or standard Darcy–Bénard) dispersion relation as given above. The latter expression cannot be rearranged into a form whereby Ra is given explicitly in terms of k, and therefore computational methods which are described later have to be used. Eq. (35) shows that there are two families of curves when there are two sublayers.

The corresponding dispersion relation for three sublayers was also derived analytically and found to be the product of three factors. Thus neutral stability corresponds to when the following are satisfied:

$$\begin{aligned} &\sin\sigma = 0, \\ &\text{or} \quad \lambda\sin\sigma(\cosh\lambda + \tfrac{1}{2}) + \sigma\sinh\lambda(\cos\sigma + \tfrac{1}{2}) = 0, \\ &\text{or} \quad \lambda\sin\sigma(\cosh\lambda - \tfrac{1}{2}) + \sigma\sinh\lambda(\cos\sigma - \tfrac{1}{2}) = 0. \end{aligned} \tag{36}$$

For three sublayers we see that there are three families of curves. Details of these families will be discussed in the next section.

It may be noted that the dispersion relations for both two and three sublayers given above may be written in a general form. Thus either $\sin\sigma = 0$, or else

$$\lambda\sin\sigma[\cosh\lambda - \cos(j\pi/N)] + \sigma\sinh\lambda[\cos\sigma - \cos(j\pi/N)] = 0, \tag{37}$$

for $j = 1, \ldots, N-1$, for a system of N sublayers. Indeed, this formula also applies for $N > 3$, a fact which we were able to confirm numerically for all $N \leqslant 10$ and for $N = 20$ by comparison with the matrix-based procedure described above.

4. Numerical method

Two numerical procedures were followed to obtain the neutral curves and their respective minima. First, the curves themselves were obtained by means of finding the zero contour of the dispersion relation (be it an explicit definition, as given above, or the matrix-based computational method) on a very fine grid of values of Ra and k; such a procedure was used by Rees and Bassom [16] for convection in inclined layers. In all cases we found that the neutral curves have a single well-defined minimum. Then, second, those minima were obtained by adapting a Newton–Raphson scheme, as follows.

A straightforward Newton–Raphson scheme may be created to evaluate values of Ra for *chosen* values of k – in such cases the dispersion relation may be written in the form, $\mathcal{F}(\mathrm{Ra}, k) = 0$, and the iteration scheme is, simply,

$$\mathrm{Ra}_{m+1} = \mathrm{Ra}_m - \left.\frac{\mathcal{F}}{\partial\mathcal{F}/\partial\mathrm{Ra}}\right|_{\mathrm{Ra}_m, k}, \tag{38}$$

where the subscript, m, denotes the iteration number. At a minimum in the neutral curve both $\mathcal{F} = 0$ and $\partial\mathcal{F}/\partial k = 0$ are satisfied, and this extra condition enables us to find the value of k. The new iteration scheme is,

$$\begin{pmatrix} \mathrm{Ra}_{m+1} \\ k_{m+1} \end{pmatrix} = \begin{pmatrix} \mathrm{Ra}_m \\ k_m \end{pmatrix} - \begin{pmatrix} \frac{\partial\mathcal{F}}{\partial\mathrm{Ra}} & \frac{\partial^2\mathcal{F}}{\partial\mathrm{Ra}\,\partial k} \\ \frac{\partial\mathcal{F}}{\partial k} & \frac{\partial^2\mathcal{F}}{\partial k^2} \end{pmatrix}^{-1} \begin{pmatrix} \mathcal{F} \\ \frac{\partial\mathcal{F}}{\partial k} \end{pmatrix}. \tag{39}$$

This method was implemented using a simple numerical differentiation procedure to evaluate the derivatives in the iteration matrix,

which, given the complexity of the definition of $\mathcal{F}$, is substantially quicker than by attempting to find the derivatives analytically.

5. Results and asymptotic analyses

5.1. Neutral curves and profiles

Fig. 2 shows a selection of neutral curves for 2, 3, 5, and 10 sublayers. These curves show a number of distinctive features which will be discussed in turn. Clearly they all have the classical shape of having only one minimum and they satisfy $\mathrm{Ra} \to \infty$ as $k \to 0$ and as $k \to \infty$.

The principal and most striking observation gained from Fig. 2 is that, when there are N sublayers, the neutral curves tend to collect together into groups of N curves; this is seen most effectively when $N = 10$ in Fig. 2. In each group the uppermost curve corresponds to a single-layer Darcy–Bénard mode. More specifically, mode nN for the present multilayer system corresponds to mode n of the single-layer Darcy–Bénard system, and these curves are given by Eq. (20). Below each of these Darcy–Bénard curves lie $N - 1$ other curves, and they correspond to the dispersion relation given by Eq. (37) where $j = 1$ corresponds to the lowest curve in each group.

Fig. 3 displays the first 10 neutral mode profiles for the case of 5 sublayers where the wavenumbers for each correspond to the minimum in the respective neutral curve. Concentrating first on the first 5 modes, the temperature profile for mode 1 looks very much like a slightly wavy version of a half sine wave, while mode 2 is a similar version of a full sine wave, and so on. The corresponding streamfunction profiles, on the other hand, are constrained greatly by the presence of the interfaces as they have to take a zero value at those places. Mode 1 consists of five curves, each of which is close to being half sine waves, but where the amplitudes increase towards the middle sublayer and then decrease once more. In practice, this pattern corresponds to a vertically stacked system of

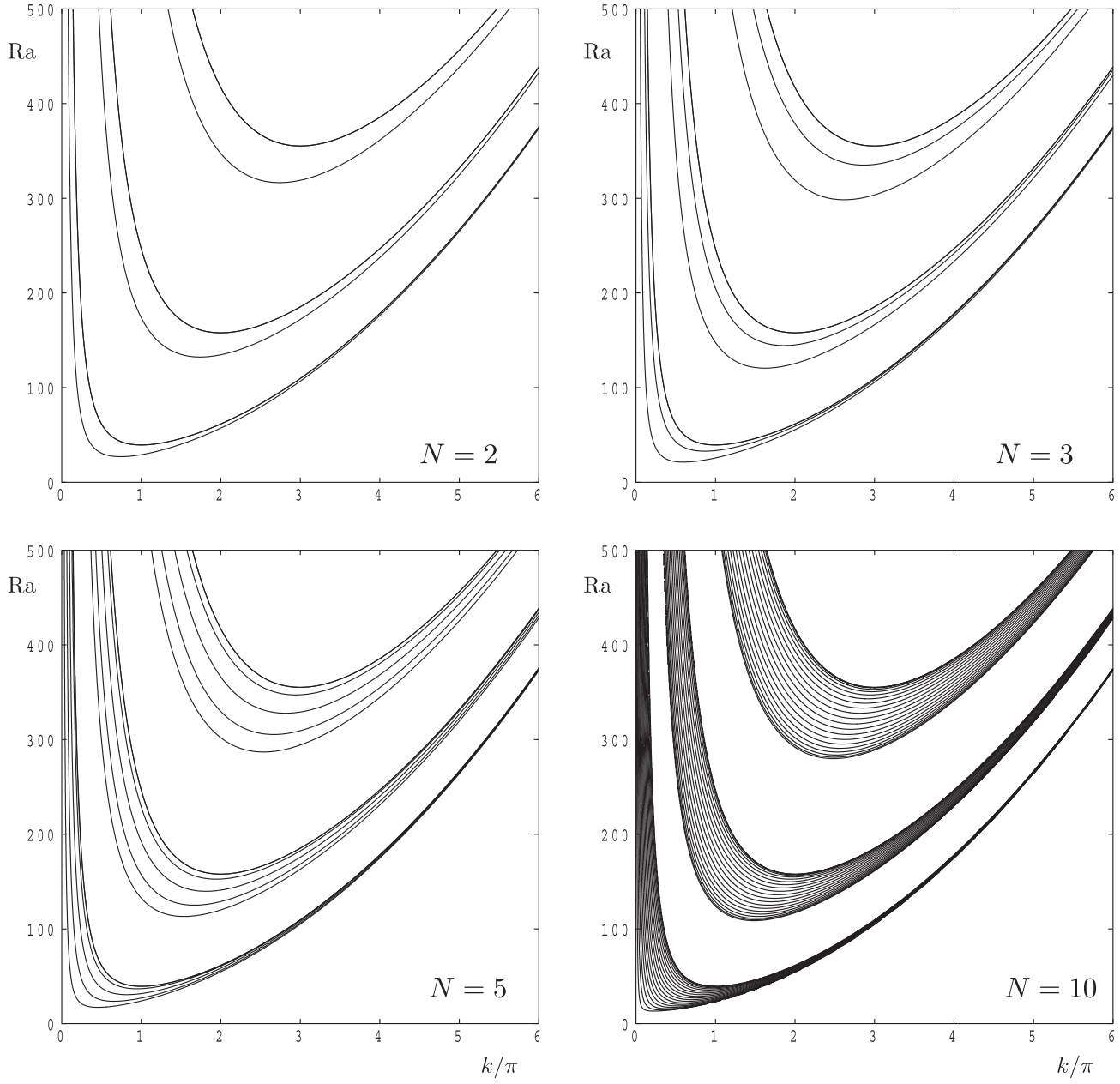

Fig. 2. The neutral curves corresponding to the first $3N$ modes of instability for N sublayers, where $N = 2$, 3, 5 and 10.

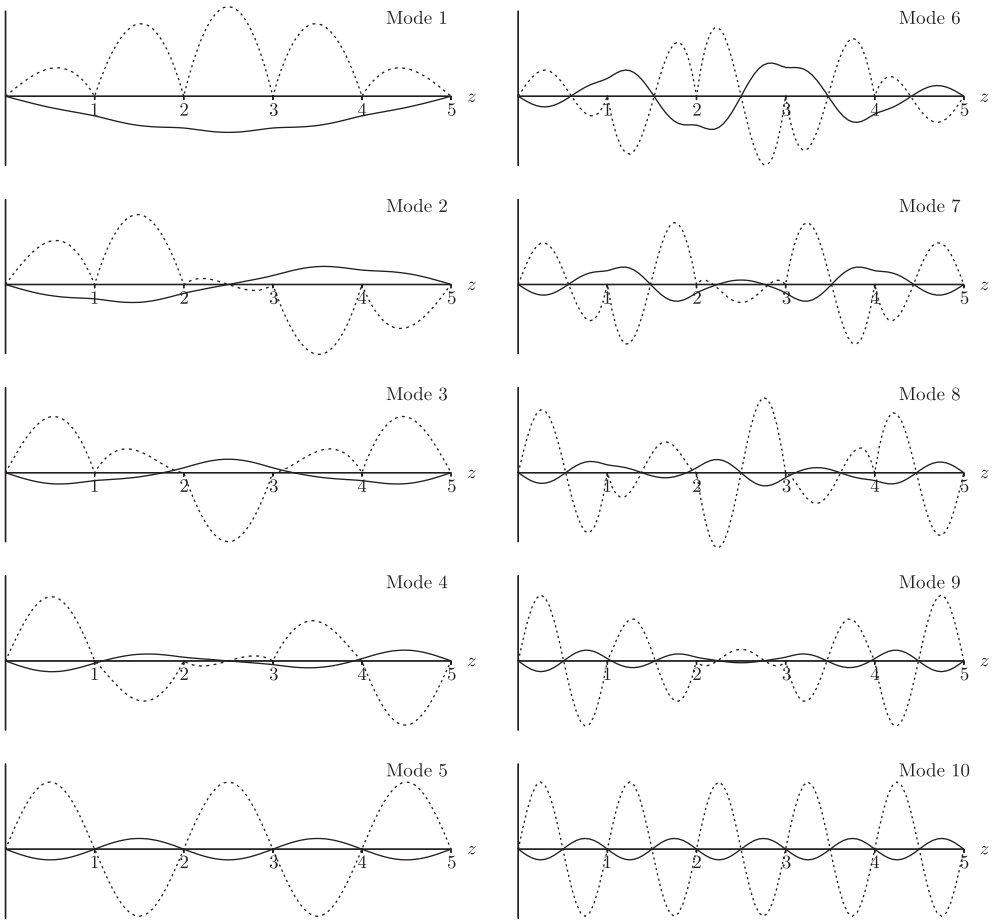

Fig. 3. Profiles of the reduced streamfunction, $f(z)$ (dashed lines), and the reduced temperature, $g(z)$ (continuous lines), for modes 1–10 for $N = 5$ sublayers.

co-rotating cells and arises irrespective of the number of sublayers. This system bears some similarity to a counter-flow heat exchanger because the flow either side of each interface is in the opposite direction, and the temperature gradient at the interface is small relative to that within the bulk of the sublayer. Mode 2 has the property that sublayers 1 and 2 contain corotating cells, that sublayers 4 and 5 also have corotating cells but whose direction of circulation is opposite to that in sublayers 1 and 2, while sublayer 3, the central sublayer, contains a stacked pair of weakly contrarotating cells. Mode 5, which is a Darcy–Bénard mode, consists of identical vertically stacked contrarotating cells.

The chief difference between modes 1–5 and modes 6–10 lies in the fact that each sublayer generally contains a single cell for the first set of five and a pair of contrarotating cells for the second set. This, perhaps, is a reason why the modes split into natural groups of five, or, more generally, into groups of N modes when there are N sublayers.

When N is odd, we may make very similar observations to those in the last-but-one paragraph. The comment on mode 1 remains the same, while mode 2 consists of two sets of corotating cells in the upper and lower halves of the layer, while the central sublayer, namely sublayer $\frac{1}{2}(N+1)$ still has the pair of counter-rotating cells. The Darcy–Bénard layer with its identical counter-rotating cells is now mode N. When N is even similar observations also apply, except that mode 2 now consists of one set of corotating cells in sublayers 1 to $N/2$ and a second set of corotating cells in the remaining sublayers, albeit with the opposite circulation to the first set.

Fig. 4 shows the variation in the temperature profiles for mode 1 for different values of N. Once more we see the fact that the overall shape is that of a half sine wave. The corresponding streamfunction profiles are omitted for the sake of brevity, but they may be caricatured well by the function, $|\sin \pi z| \sin(\pi z/N)$.

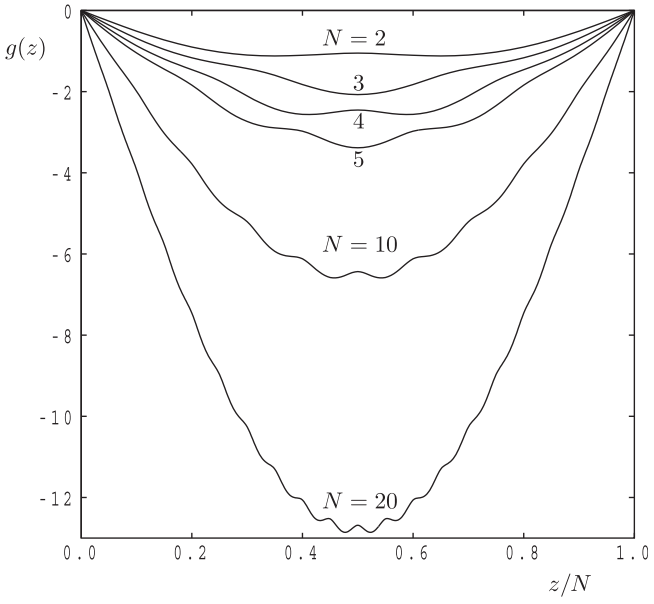

Fig. 4. Reduced temperature profiles for $N = 2, 3, 4, 5, 10$ and 20 as a function of z/N. The curves correspond to where $\mathrm{Ra} = \mathrm{Ra}_c$ and $k = k_c$.

5.2. Analysis for large values of k

Fig. 2 also shows that each group of N curves tends towards a common curve as the wavenumber, k, increases. This is most obvious for the lowest group of curves in each case, but our computations (not shown) for larger values of k show this very clearly. This behaviour may be confirmed by performing an asymptotic analysis of the dispersion relation given in Eq. (37).

Beginning with Eq. (37), we set both $\mathrm{Ra} \gg 1$ when $k \gg 1$. In turn this means that $\lambda \gg 1$ and hence that $\sinh\lambda \sim \cosh\lambda$ with an exponentially small error. Therefore we may replace Eq. (37) by,

$$\lambda \sin\sigma + \sigma[\cos\sigma - \cos(j\pi/N)] = 0. \tag{40}$$

We already know that $\mathrm{Ra} = k^2 + 2\pi^2 + k^{-2}$ for the Darcy–Bénard mode, which is exactly equivalent to $\sigma = \pi$. Therefore the second term in Eq. (40) is of $O(1)$ magnitude. Given that $\lambda = O(k)$, we need $\sin\sigma = O(k^{-1})$ to render the first term in Eq. (40) to be of $O(1)$ magnitude too. This may be achieved by setting,

$$\mathrm{Ra} = k^2 + 2\pi^2 + ck^{-1} + O(k^{-2}), \tag{41}$$

because it yields $\sigma = \pi + O(k^{-1})$, as required. Substitution of the above expression for Ra into the definitions of λ and σ and their subsequent substitution into Eq. (40) give the following expression at leading order,

$$-\frac{\sqrt{2}c}{4\pi} + \pi[-1 - \cos(j\pi/N)] = 0. \tag{42}$$

Therefore we have

$$c = -2\sqrt{2}\pi^2[1 + \cos(j\pi/N)], \tag{43}$$

and hence,

$$\mathrm{Ra} \sim k^2 + 2\pi^2 - \left[2\sqrt{2}\pi^2[1 + \cos(j\pi/N)]\right]k^{-1}, \tag{44}$$

for $j = 1, \ldots, N-1$. This latest expression is valid only for the first group of N curves for a general N-sublayer configuration. Therefore the individual curves comprising the first group lie at an $O(k^{-1})$ distance from one another when k is large. A similar analysis may be undertaken to show that such a conclusion is also true for other groups, although each group lies at an $O(1)$ distance from any other group.

5.3. Critical values of Ra and k

Physically, the most important value of Ra is the one which corresponds to the minimum point of the neutral curve for the first mode. This value will be denoted by Ra_c and linear theory predicts that all disturbances decay when $\mathrm{Ra} < \mathrm{Ra}_c$. The value of k at which $\mathrm{Ra} = \mathrm{Ra}_c$ is denoted by k_c and it is called the critical wavenumber. In addition we define Ra_{cj} to correspond to the minimum value of Ra for mode j, and therefore $\mathrm{Ra}_c = \mathrm{Ra}_{c1}$.

A good idea of how the values of Ra_{cj} and k_{cj} vary with N and j may be gleaned from Fig. 2, but a much clearer view is given in Figs. 5 and 6 where we show the dependence of these values on $1/N$ for the first N modes. In both figures the values for mode N are the largest values displayed and they take the classical Darcy–Bénard values of $4\pi^2$ and π, respectively. Of more interest are the lowest values which correspond to mode 1. Fig. 5 appears to suggest that Ra_c is approaching a value close to 12 as N increases. On the other hand, it is a little more difficult to discern what is happening in Fig. 6, but it looks as though k_c might be approaching 0 as a function of $N^{-1/2}$.

In Table 1 we display the values of Ra_c and k_c for different values of N, where the data is correct to the given number of significant figures. Further columns in that table show the results of processing that raw data.

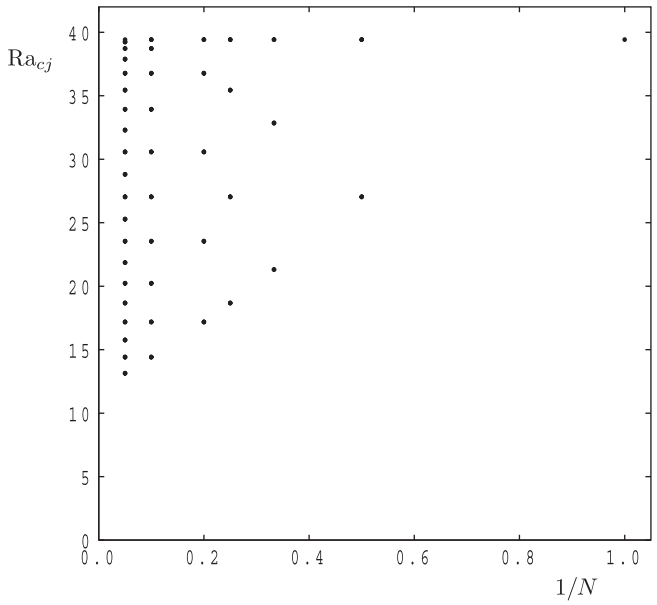

Fig. 5. Values of Ra_{cj} as a function of $1/N$. For each value of N we show Ra_{cj} for $j = 1$ (lowest) to $j = N$ (highest).

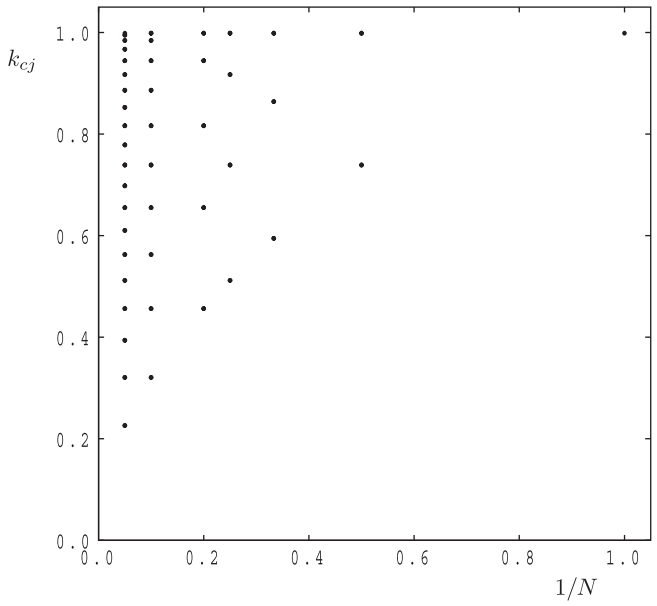

Fig. 6. Values of k_{cj} as a function of $1/N$. For each value of N we show k_{cj} for $j = 1$ (lowest) to $j = N$ (highest).

Table 1
Values of Ra_c and k_c for various numbers of sublayers, together with data from which asymptotic expansions for $N \gg 1$ will be derived.

N	Ra_c	$N(\mathrm{Ra}_c - 12)$	k_c/π	$N^{1/2}k_c/\pi$
5	17.236333	26.1817	0.457578	1.02318
10	14.471082	24.7108	0.322080	1.01851
20	13.199202	23.9840	0.227374	1.01685
40	12.590616	23.6246	0.160671	1.01617
80	12.293076	23.4461	0.113578	1.01587
160	12.145982	23.3571	0.080301	1.01574
320	12.072852	23.3126	0.056777	1.01566

Table 1 demonstrates clearly that $\mathrm{Ra}_c \to 12$ and $k_c \to 0$ as $N \to \infty$. This suggests that the present multilayered problem in

the large-N limit might display some relationship to the single-layer constant-heat-flux form of the Darcy–Bénard problem (which we shall abbreviate to CHFDB1) which has exactly the same critical values. As a first step in investigating such a possibility, neutral curves for mode 1 for various values of N have been plotted in Fig. 7 together with that for mode 1 for the CHFDB1 problem.

Fig. 7 indicates firstly that, for a chosen value of k, the multilayer neutral curves clearly approach that for the CHFDB1 problem as N increases. However, that convergence is not uniform because the neutral curve for any chosen value of N, however large, rises to infinity when k is sufficiently small, whereas the curve for the CHFDB1 problem tends toward 12 as $k \to 0$. These two aspects will be dealt with in turn in the next two subsections.

Given that the asymptotic limit of $N \to \infty$ reproduces the critical parameters which are usually associated with the application of constant heat flux boundary conditions on a single porous layer, it is natural to ask if there are any physical reasons why there is a connection between the two problems. For a large number of sublayers, particularly if one views the overall layer as a system with narrow sublayers, the porous medium becomes strongly anisotropic and fluid is able to flow more easily in the horizontal direction but there remains a relatively weak vertical velocity in order to maintain an overall circulation within each sublayer. Given the presence of this almost parallel flow one ought to have had an a priori expectation that the critical mode has a wavelength which is much larger than the height of a sublayer. An examination of the $N = 20$ case shown in Fig. 4 also reveals the fact that the temperature gradient at the interfaces is substantially smaller than that found within the interior of a sublayer, particularly when that sublayer is near the middle of the layer. Therefore interior sublayers are approximate versions of the CHFDB1 problem, with the approximation becoming less valid as the upper and lower boundaries of the layer are approached.

5.4. Asymptotic analysis for $N \gg 1$ for fixed values of k

In this subsection we focus on the limiting case of a large number of sublayers for fixed values of k. This task is made relatively straightforward by the existence of the dispersion relation given in Eq. (37). We already know that the first mode is given by $j = 1$ in Eq. (37), and therefore, as $N \to \infty$, the multilayer dispersion relation for mode 1 becomes

$$\lambda \sin\sigma[\cosh\lambda - 1] + \sigma \sinh\lambda[\cos\sigma - 1] = 0. \tag{45}$$

On the other hand, the dispersion relation for the CHFDB1 problem may be shown easily to take the form,

$$k^2 \sinh\lambda \sin\sigma + \lambda\sigma(\cos\sigma\cosh\lambda - 1) = 0. \tag{46}$$

These two expressions look very different, and therefore we plotted the neutral curves corresponding to each, and found that the respective odd-numbered modes (1st, 3rd and so on) were identical to within round-off accuracy, but the even-numbered modes were quite different from one another. This unusual behaviour may be explained by the fact that Eqs. (45) and (46) may both be factorised. Thus Eq. (45) may be written in the form,

$$\sin\sigma/2 \sinh\lambda/2[\lambda\cos\sigma/2\sinh\lambda/2 - \sigma\sin\sigma/2\cosh\lambda/2] = 0, \tag{47}$$

while Eq. (46) may be written in the form,

$$[\sigma\cos\sigma/2\sinh\lambda/2 - \sigma\sin\sigma/2\cosh\lambda/2][\lambda\cos\sigma/2\sinh\lambda/2 - \sigma\sin\sigma/2\cosh\lambda/2] = 0. \tag{48}$$

These expressions have a common factor, and it is this factor which corresponds to the odd-numbered modes for each of the separate problems and, in particular, for the first mode. Therefore we may conclude that, for fixed values of k, we recover the neutral curve for the single-layer constant heat flux Darcy–Bénard problem when we have an asymptotically large number of sublayers.

5.5. Asymptotic analysis of Ra_c and k_c when $N \gg 1$

We now address the detailed behaviour of Ra_c and k_c as $N \to \infty$. The analysis is assisted greatly by the behaviour of some of the data shown in Table 1, which suggests that $Ra_c \simeq 12 + 12.3N^{-1}$ and $k_c \simeq 1.106\pi N^{-1/2}$. The quantity, $\cos(j\pi/N)$, which occurs in the dispersion relation, (37), is approximated by $1 - \pi^2/2N^2$ when $j = 1$ and $N \gg 1$. Therefore, we shall define the small quantity, δ, according to,

$$\delta = N^{-1/2}. \tag{49}$$

Given that both λ and σ are now small quantities, the expansion of the dispersion relation, Eq. (37), is facilitated by first expanding in terms of λ and σ. Therefore we may approximate,

$$\lambda\sin\sigma\left[\cosh\lambda - 1 + \frac{1}{2}\pi^2\delta^4\right] + \sigma\sinh\lambda\left[\cos\sigma - 1 + \frac{1}{2}\pi^2\delta^4\right] = 0, \tag{50}$$

by the following,

$$\lambda\sigma\left[\left(1 - \frac{\sigma^2}{6} + \frac{\sigma^4}{120} - \frac{\sigma^6}{5040} + \cdots\right)\left(\frac{\lambda^2}{2} + \frac{\lambda^4}{24} + \frac{\lambda^6}{720} + \frac{\lambda^8}{40320} + \cdots + \frac{\pi^2\delta^4}{2}\right) + \left(1 + \frac{\lambda^2}{6} + \frac{\lambda^4}{120} + \frac{\lambda^6}{5040} + \cdots\right)\left(-\frac{\sigma^2}{2} + \frac{\sigma^4}{24} - \frac{\sigma^6}{720} + \frac{\sigma^8}{40320} + \cdots + \frac{\pi^2\delta^4}{2}\right)\right] = 0. \tag{51}$$

The terms in the square brackets may eventually be simplified to the form,

$$k^2 - \frac{k^2\mathrm{Ra}}{2} + k^4\left(\frac{1}{4} - \frac{\mathrm{Ra}}{72} + \frac{\mathrm{Ra}^2}{12096}\right) + \pi^2\delta^4 + O(k^6) = 0. \tag{52}$$

If we now substitute the quantities,

$$\mathrm{Ra} = 12 + S\delta^2, \quad k = \hat{k}\delta, \tag{53}$$

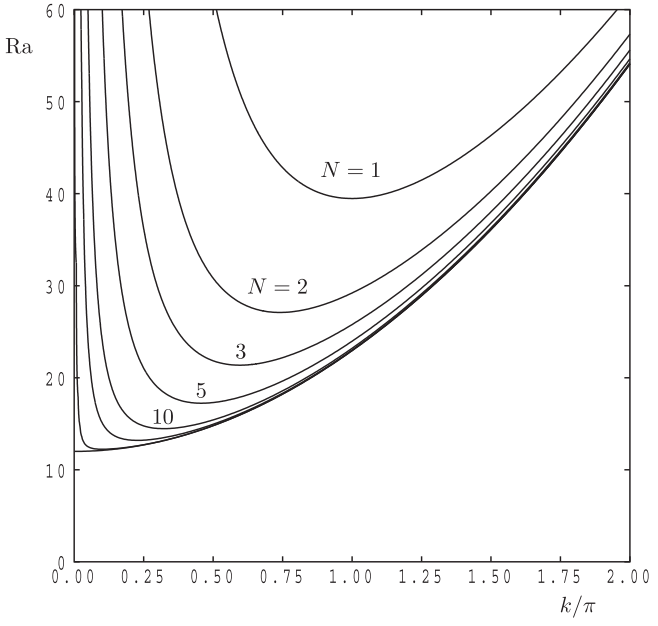

Fig. 7. Neutral curves displaying values of Ra as functions of k for mode 1, for $N = 1$ (the Darcy–Bénard layer), 2, 3, 5, 10, 20 and 100. Also shown is the neutral curve for mode 1 of the CHFDB1 problem, which is exact equivalent to the limit, $N \to \infty$; this curve takes the value, 12, when $k = 0$.

then the $O(\delta^2)$ terms cancel, and the coefficients of δ^4 yield

$$S = \frac{12\pi^2}{\hat{k}^2} + \frac{8\hat{k}^2}{7}. \tag{54}$$

The second term in Eq. (54) corresponds to the second term in the small-k expansion of the neutral curve for the CHFDB1 problem, namely that $\mathrm{Ra}_c \sim 12 + \frac{8}{7}k^2$. The first term, however, is the one that is responsible for the present $N \gg 1$ neutral curves ascending to infinity as $k \to 0$.

We may now use Eq. (54) to determine the behaviour of Ra_c and k_c as $N \to \infty$. Setting to zero the derivative of S with respect to $\hat{k}$ yields,

$$\hat{k} = \left(\frac{21}{2}\right)^{1/4} \pi^{1/2} = 1.0155993\pi, \tag{55}$$

and the corresponding value of S is

$$S = 24\left(\frac{2}{21}\right)^{1/2} \pi^2 = 23.268397. \tag{56}$$

Therefore we conclude that the critical values of Ra and k have the following leading order form,

$$\mathrm{Ra}_c \sim 12 + 23.268397N^{-2}, \quad k_c \sim 1.1055993\pi N^{-1/2}, \tag{57}$$

as $N \to \infty$, both of which compare very well indeed with the data presented in Table 1. Therefore, when $N \gg 1$, there are three disparate length scales which apply to the layer: the layer has thickness N, the sublayer has height 1, and the horizontal extent of one convection cell corresponding to the most unstable mode has length $N^{1/2}/1.0155993$.

6. Conclusion

In this paper we have given a comprehensive analysis of the onset of convection in a multiply-layered systems where each sublayer is (i) identical in all respects and (ii) separated by a infinitesimally thin impermeable interface. Dispersion relations for two and three sublayers have been obtained, and simple numerical procedure described for an arbitrary number of sublayers. By examining the form of the dispersion relations for two and three sublayers, a simple analytical expression for general values of N has been obtained; see Eq. (37). Some typical onset profiles have been presented and described. Detailed numerical and asymptotic analyses have been presented which (i) explains the bunching characteristic of the neutral curves when k is large, (ii) explains the approach to the single-layer constant-heat-flux neutral curve as $N \to \infty$, and (iii) determines the values of Ra_c and k_c as $N \to \infty$.

Acknowledgements

The second author (G.G.) wishes to thank the Erciyes University Foundation for supporting this work with a research fellowship, and the University of Bath for their hospitality.The authors would also like to thank Prof. P.A. Tyvand for interesting discussions and for his assistance.

References

[1] G. Genç, D.A.S. Rees, Onset of convection in horizontally partitioned porous layers, Physics of Fluids, submitted for publication.
[2] St.I. Georghitza, The marginal stability in porous inhomogeneous media, Proc. Camb. Phil. Soc. 57 (1961) 871–977.
[3] I.G. Donaldson, Temperature gradients in the upper layers of the earth's crust due to convective water flows, J. Geophys. Res. 67 (1962) 3449–3459.
[4] D.N. Riahi, Nonlinear convection in a porous layer with finite conducting boundaries, J. Fluid Mech. 129 (1983) 153–171.
[5] A. Mojtabi, D.A.S. Rees, The onset of the convection in Horton–Rogers–Lapwood experiments: the effect of conducting bounding plates, Int. J. Heat Mass Transfer 54 (2011) 293–301.
[6] D.A.S. Rees, A. Mojtabi, The effect of conducting boundaries on weakly nonlinear Darcy–Bénard convection, Transp. Porous Media (2011).
[7] T. Masuoka, T. Katsuhara, Y. Nakazono, S. Isozaki, Onset of convection and flow patterns in a porous layer of two different media, Heat Transfer: Japan. Res. 7 (1979) 39–52.
[8] R. Rana, R.N. Horne, P. Cheng, Natural convection in a multi-layered geothermal reservoir, ASME C: J. Heat Transfer 101 (1979) 411–416.
[9] R. McKibbin, M.J. O'Sullivan, Onset of convection in a layered porous medium heated from below, J. Fluid Mech. 96 (1980) 375–393.
[10] R. McKibbin, M.J. O'Sullivan, Heat transfer in a layered porous medium heated from below, J. Fluid Mech. 111 (1981) 141–173.
[11] R. McKibbin, P.A. Tyvand, Thermal convection in a porous medium with horizontal cracks, Int. J. Heat Mass Transfer 27 (1984) 1007–1023.
[12] R. McKibbin, P.A. Tyvand, Thermal convection in a porous medium composed of alternating thick and thin layers, Int. J. Heat Mass Transfer 26 (1983) 761–780.
[13] J.Y. Jang, W.L. Tsai, Thermal instability of two horizontal porous layers with a conductive partition, Int. J. Heat Mass Transfer 31 (1988) 993–1003.
[14] A. Postelnicu, Thermal stability of two fluid porous layers separated by a thermal barrier, Proceedings of the 3rd Baltic Heat Transfer Conference, Gdansk, Poland, 22–24 September 1999, pp. 443–450.
[15] D.A.S. Rees, D.S. Riley, The three-dimensional stability of finite-amplitude convection in a layered porous medium heated from below, J. Fluid Mech. 211 (1989) 437–461.
[16] D.A.S. Rees, A.P. Bassom, Onset of Darcy–Bénard convection in an inclined porous layer heated from below, Acta Mechanica 144 (2000) 103–118.